

# Magnetic Nanocarriers Enhance Drug Delivery Selectively to Human Leukemic Cells

Kheireddine El-Boubbou<sup>1,2\*\*</sup>, Rizwan Ali<sup>2#</sup>, Hassan M Bahhari<sup>2</sup> and Mohamed Boudjelal<sup>2</sup>

<sup>1</sup>Department of Basic Sciences, King Saud bin Abdulaziz University for Health Sciences (KSAU-HS), King Abdulaziz Medical City, National Guard Health Affairs, Riyadh 11481, Saudi Arabia

<sup>2</sup>Department of Basic Sciences, King Abdullah International Medical Research Center (KAIMRC), King Abdulaziz Medical City, National Guard Hospital, Riyadh 11426, Saudi Arabia

\*Kheireddine El-Boubbou and Rizwan Ali contributed equally

## Abstract

Selective drug delivery to human leukemia cells using a nanoparticulate chemotherapeutic formulation is hugely needed. In this work, we report the development of a magnetic nanocarrier made of PVP-stabilized magnetic iron oxide nanoparticles (PMNP) loaded with the anticancer drug Doxorubicin (Dox) as a promising selective drug carrier to different types of human leukemia and normal cells. Our results revealed that while the unloaded MNPs were not potent to any of the cells, Dox@PMNPs showed significant toxicities, effectively killing the different leukemia cells, albeit at different inhibitory concentrations. Interestingly and superior to free Dox, Dox@PMNPs showed enhanced and significant inhibition towards the human monocytic THP-1 cells compared to human promyelocytic leukemia cells HL-60 (2-fold enhanced cytotoxicities), with the least potency towards the normal peripheral blood mononuclear cell (PBMC) cells (up to 6-fold). Nonetheless, free Dox was found to be concurrently less toxic to all the three cell lines tested. The cytotoxic effects obtained were further confirmed by live confocal imaging and electron microscopy. Both imaging techniques confirmed distinct morphological changes (membrane blebbing, shrinkage, and condensation) corresponding to typical apoptotic features in the treated leukemia cells compared to normal PBMC cells. The observed enhanced cytotoxic effects of Dox@PMNPs is mostly dependent upon the selective and differential endocytic uptake of Dox@PMNPs, with subsequent release of Dox intracellularly to the cytoplasm after 6 h, which then translocates to the nucleus after 24 h, causing apoptotic cell death. Importantly, magnetic Dox nanocarrier described here reduces the unwanted diffusive side effects of the free drug and allows selective drug delivery to leukemic cells, allowing its potential use for leukemic patients' theranostics.

**Keywords:** Magnetic nanoparticles; Drug delivery; Human leukemia cells; Iron oxide; Cancer nanotherapy

## Introduction

Doxorubicin (Dox) is one of the most studied chemotherapeutic anticancer drugs used for the treatment of a wide range of solid tumors and hematological malignancies (i.e. leukemia and lymphoma) in clinical practice [1,2]. This anthracycline drug is isolated from the culture of *Streptomyces peucetius* and administered intravenously as the hydrochloride salt during therapy. However, the cardiotoxicity and poor selectivity of this drug limits its direct administration and cumulative dosage resulting in off-target side effects. Hence, without changing the drug itself, there is a great incentive to develop alternative, rapid and more effective chemotherapeutic approaches to direct the drug to its target [3]. Consequently, different Dox formulations and modifications that allow it to evade membrane transporters have been the subject of many new formulations, many of them are nano-based [4-8]. Particularly, special attention have been devoted to the significant role of magnetic iron oxide nanoparticles (MNPs) in enhancing intracellular drug uptake/anticancer drug accumulation inducing apoptotic cell death, and offering means to inhibit the cellular drug resistance, thus providing promising imaging/targeting potentials in leukemia therapy [9-12].

MNPs have been extensively studied not only as imaging vehicles, but also as drug nanocarriers [13-16]. The main advantages of using MNPs for such purposes are: 1) easy preparation; 2) small sizes and large surface areas; 3) facile chemical functionalization; 3) excellent biocompatibility and stability; 4) efficient drug conjugation; and 5) superior magnetic responsiveness. Such unique properties of MNPs enabled their use as MRI contrast agents, hyperthermia agents, magnetic field guided localization vectors, and/or drug delivery

vehicles [17]. Hence, MNPs are excellent candidates for targeted drug delivery and image-guided therapeutics with a great potential in clinical cancer theranostics [18,19]. Although there are many reports on the utilization of drug-loaded MNPs for cancer imaging and therapy [20-24], very few reports have focused on human leukemic cancer [9-12,25-29]. Moreover, all of these studies are focused on only one type of leukemia cells K562 derived from chronic myelogenous leukemia (CML) patients.

Leukemia, a malignant progressive devastating cancer of the blood cells, is caused by the replacement of normal white blood cells with immature or abnormal leukemic cells, with limited treatment strategies possibly due to poorly effective drug delivery to affected areas [30]. Unlike solid tumors, leukemic patients can't be cured by surgical treatment. The main strategy for treatment is using chemotherapy. Although many different clinical antitumor agents are currently used in the treatment of acute promyelocytic leukemia (APL), acute myeloid leukemia (AML), or CML patients, a high proportion of these leukemic patients eventually relapse [31-33]. Hence, alternative approaches

\*Corresponding author: Kheireddine El-Boubbou, King Saud bin Abdulaziz University for Health Sciences (KSAU-HS), King Abdulaziz Medical City, National Guard Health Affairs, Riyadh 11481, Saudi Arabia, Tel: 966 1142995625; Fax: 9661142995340; E-mail: [elboubboukh@ngha.med.sa](mailto:elboubboukh@ngha.med.sa)

Received: May 02, 2017; Accepted: May 16, 2017; Published: May 23, 2017

Citation: El-Boubbou K, Ali R, Bahhari HM, Boudjelal M (2017) Magnetic Nanocarriers Enhance Drug Delivery Selectively to Human Leukemic Cells. J Nanomed Nanotechnol 8: 441. doi: [10.4172/2157-7439.1000441](https://doi.org/10.4172/2157-7439.1000441)

Copyright: © 2017 El-Boubbou K, et al. This is an open-access article distributed under the terms of the Creative Commons Attribution License, which permits unrestricted use, distribution, and reproduction in any medium, provided the original author and source are credited.

employing delivery systems that tends to improve therapeutic targeting, enhance the drug efficacy, and reduce the systemic side effects of chemotherapeutic drugs are being actively sought.

We specifically focused on drug delivery to two human leukemic cell lines THP-1 and HL-60, as well as human peripheral blood mononuclear cells (PBMCs) as controls. These different cell lines are anticipated to have different characteristics, endocytic potentials, and response to chemotherapy. THP-1 is a human monocytic cell line derived from an acute monocytic leukemic patient. THP-1 is single, round cells with distinct monocytic markers resembling primary monocytes and macrophages in morphology, function and differentiation properties [34]. After exposure to phorbol-12-myristate-13-acetate (PMA), nearly all the THP-1 cells start to adhere to culture plates accompanied by differentiation into a macrophage phenotype with marked morphological changes [35]. On the other hand, HL-60, a human promyelocytic leukemia cell line, was derived from a patient with AML, and is typically used as an attractive model for studying human myeloid cell proliferation and differentiation [36].

In this work, the utilization of Dox-loaded polymer-stabilized MNPs (Dox@PMNPs) as effective and selective drug delivery vehicles for the different leukemic cells was evaluated. Systematic toxicities and inhibitory concentrations against the different types of cells were evaluated. Moreover, live confocal and electron microscopy were conducted to investigate the intracellular NP trafficking and drug release properties inside the cells. Importantly, to our knowledge, this is the first report using nanoparticulate drug nanocarriers to systematically study the selective delivery of cytotoxic agents to human leukemic cancer cells. Importantly, the MNP formulation developed here can potentially open new opportunities for *in vivo* leukemia therapeutic imaging and hyperthermia.

## Experimental Section

### Materials, methods and cell lines

Unless otherwise indicated, all chemicals and solvents were obtained from commercial suppliers and used as supplied without further purification. Iron (III) chloride hexahydrate ( $\text{FeCl}_3 \cdot 6\text{H}_2\text{O}$ ), iron (II) chloride tetrahydrate ( $\text{FeCl}_2 \cdot 4\text{H}_2\text{O}$ ), doxorubicin (Dox), and the polymer Poly-N-vinylpyrrolidone (PVP) (MW=58,000) were all purchased from UFC Biotechnology. All reactions for the NP syntheses were carried under an argon atmosphere. 0.2  $\mu\text{m}$  filtered deionized water was used for the synthesis of the nanoparticles. All cell lines were purchased from the American Type Culture Collection (ATCC) and grown in RPMI 1640 medium supplemented with 10% FBS and 1% Penicillin/Streptomycin. Human leukemic cells used in this study are: THP-1 (human monocytic cell lines derived from an acute monocytic leukemia patient); HL-60 (human promyelocytic leukemia cells derived from the peripheral blood of a 36-year-old woman with AML FAB M2); and in-lab prepared human PBMCs as controls. For PBMCs, peripheral blood samples were collected from Dr. El-Boubbou's own blood at KAIMRC under approval from the institution. PBMCs were then isolated using ficoll-paque gradient as described previously. Briefly, 10 ml of drawn blood were diluted 3-fold in dilution buffer (PBS saline, 2 mM EDTA), layered carefully over ficoll-paque and centrifuged at 4500 rpm for 20 min. The layer corresponding to PBMCs was isolated, transferred to 45 ml of dilution buffer, centrifuged twice at 3000 rpm for 20 min and the resulting pellet re-suspended in 10 ml growth media. TEM images were collected on a JEOL-JEM 1230 operating at 100 kV using Gatan camera with Digital Micrograph Imaging software. SEM images were processed using a FEI NanoSEM 450 scanning electron microscope at 15 kV.

DLS measurements were assessed on Malvern Zetasizer Nano ZS instrument. TGA were carried out on a PerkinElmer TGA 4000 equipment and the samples were burned under nitrogen at a constant heating rate of  $10^\circ\text{C}/\text{min}$  from 35 to  $700^\circ\text{C}$ . Confocal microscopy images were visualized using inverted Zeiss LSM 780 multiphoton laser scanning confocal microscope equipped with 20x and 40x (oil immersion) objectives and axiocam cameras.

### Preparation of Dox@PMNPs

$\text{FeCl}_3 \cdot 6\text{H}_2\text{O}$  (30 mg, 0.11 mmol) and PVP (15 mg) were mixed in water (1 mL), followed by addition of 1 mL aqueous  $\text{FeCl}_2 \cdot 4\text{H}_2\text{O}$  (11 mg, 0.055 mmol). To the above mixture, 250  $\mu\text{L}$  Dox. HCl solution (2 mg/mL) were added, followed by addition of 2 mL  $\text{NH}_4\text{OH}$  base. The reaction mixture was stirred for 3 h at room temperature under inert argon atmosphere. The NP dispersion was then isolated *via* centrifugation (4500 rpm, 20 min), washed repeatedly (6x) with water until no Dox was detected in the supernatant, and finally redispersed in water to form stable aqueous suspensions of Dox@PMNPs (1 mg/mL NP; 67  $\mu\text{g}/\text{mL}$  Dox). Alternatively, the suspension can be dialyzed against water until no Dox is detected in the supernatant. The percentage of Dox on NPs was determined by UV-vis spectroscopy. The absorbance of the residual Dox in the supernatant was measured ( $\lambda_{\text{max}}=481$  nm) and the percentage of Dox loading (w/w%) was then quantified.

$$\text{Loading Efficiency} = \frac{W_1}{W_0} \times 100$$

The loading efficiency was calculated as:

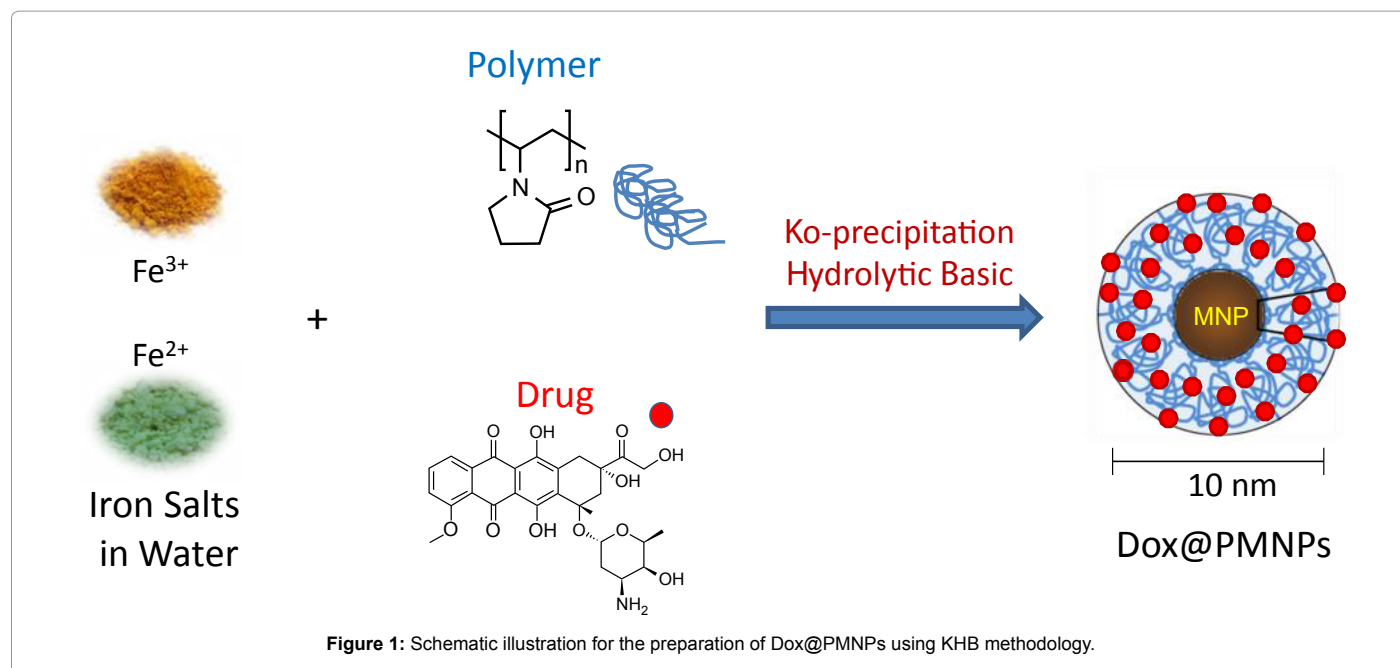
Where  $W_1$  is the amount of Dox loaded onto NPs and  $W_0$  is the weight of Dox in the initial solution. The amount of Dox adsorbed onto NPs was calculated from the difference between the initial Dox concentration and the Dox concentration in the supernatant.

### Cell viability assays

All non-adherent cells were plated in flat-bottom 96-well plates at a density of  $2-3 \times 10^5$  cells/well in 100  $\mu\text{L}$  of their respective growth medium. Serial dilutions of the different NP formulations, ranging from 50 to 0.25  $\mu\text{g}/\text{mL}$ , were made directly in the cell culture medium (RPMI+10% FBS+1% PS) performed in triplicates, and directly transferred to the cell plates containing the cells (200  $\mu\text{L}$  total volume). The wells at all edges were left free of cells in order to prevent edge effect. An additional row with only the NPs was added in order to account for the NP effect. In addition, the free drug control wells at the equivalent drug concentrations were also prepared simultaneously. After 48 h of incubation at  $37^\circ\text{C}$  with 5%  $\text{CO}_2$ , the medium was removed and the cells were washed with PBS. Cell viability was then determined using the MTT viability assay following the manufacturer's protocol. Briefly, 20  $\mu\text{L}$  of MTT reagent (5 mg/mL) was added to each well and kept for 4 h at  $37^\circ\text{C}$  in the incubator. The supernatant was then removed, and the MTT formazan was dissolved in dimethyl sulfoxide (DMSO). The absorbance was measured on iMark microplate absorbance reader at 590 nm. The percentage of viable cells was calculated as the ratio of the absorbance of the treated group divided by the absorbance of the control group multiplied by 100. The absorbance from the untreated control cells was set as 100% viable.  $\text{IC}_{50}$  values were calculated from dose-response curves generated using a polynomial dose-response approximation.

### Live confocal microscopy imaging

All non-adherent cells were suspended in the respective media in 8-well dish (Thermo-fisher Scientific) and were exposed to Dox@



PMNPs (10  $\mu\text{g}/\text{mL}$  NPs) or equivalent amount of free Dox, and further incubated for different periods of times. Hoechst 33342 stain was then added. The cells were allowed to settle down for 20 min before microscopic visualization. To mimic physiological conditions, no fixation of cells was conducted.

### Scanning electron microscopy (SEM)

Representative leukemic cells in respected buffer (2 mL) were first treated with the NPs (100  $\mu\text{g}/\text{mL}$ ) for 24 h as described above. The specimens were then processed for SEM by the following method: Cells were first fixed with 4% paraformaldehyde at 4°C and then dehydrated with graded concentrations of ethanol. The cells were then transferred to appropriate carbon taped stubs (Ted Pella, USA) for imaging. To enhance the electron conductivity, samples were coated with gold/palladium (Au/Pd) by sputter coating and examined on a FEI NanoSEM 450 scanning electron microscope at 15 kV.

### Transmission electron microscopy (TEM)

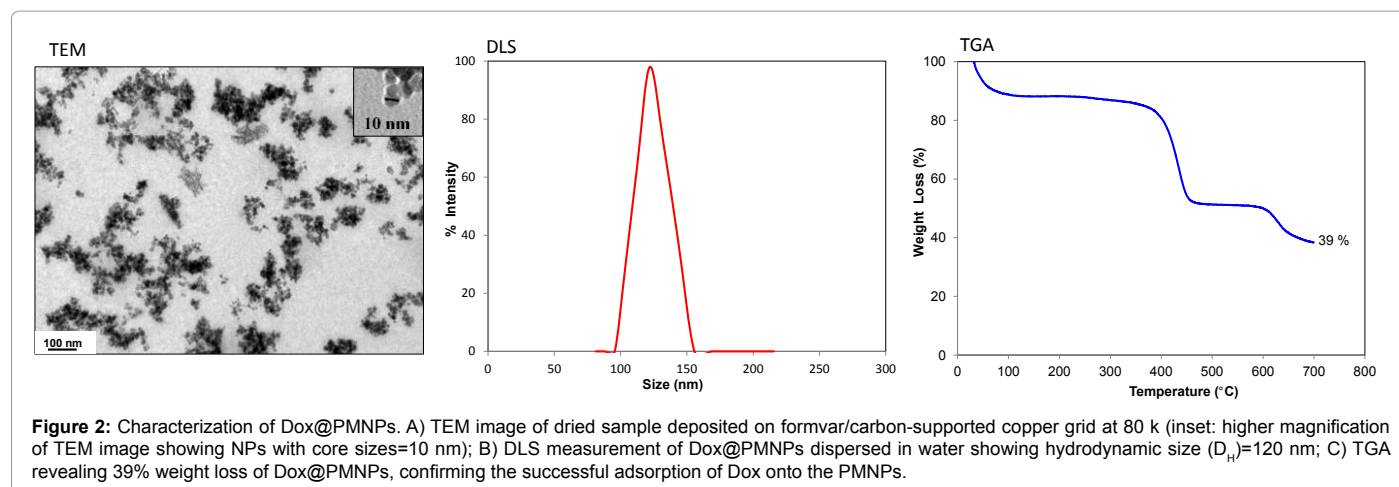
Representative leukemic cells in respected buffer (2 mL) were first treated with the NPs (100  $\mu\text{g}/\text{mL}$ ) for 24 h as described above. The specimens were then processed for TEM by the following method: the specimen was fixed in 3% glutaraldehyde in 0.1 M PBS (pH 7.4) for more than 3 h. After washing in the same buffer, this was post-fixed in 1% OsO<sub>4</sub> in 0.1 M PBS (pH 7.4) for 1 h, followed by PBS washing. The specimen was then dehydrated in a series of acetone solutions and infiltrated in ace-tone: resin (1:1) for 1 h, and then with acetone: resin (1:2) for more than 3 h. The specimen was then embedded in epoxy resin (Araldite) and placed in an oven at 80°C overnight to polymerize. Ultrathin sections were obtained with Ultra microtome (Leica EM UC6), mounted on copper grids, and stained for contrast with heavy metal stains (uranyl acetate and lead citrate). TEM images were then collected on a JEOL-JEM 1230 operating at 100 kV using Gatan camera with Digital Micrograph Imaging software.

### Result and Discussion

Dox@PMNPs used in this work were magnetic iron oxide

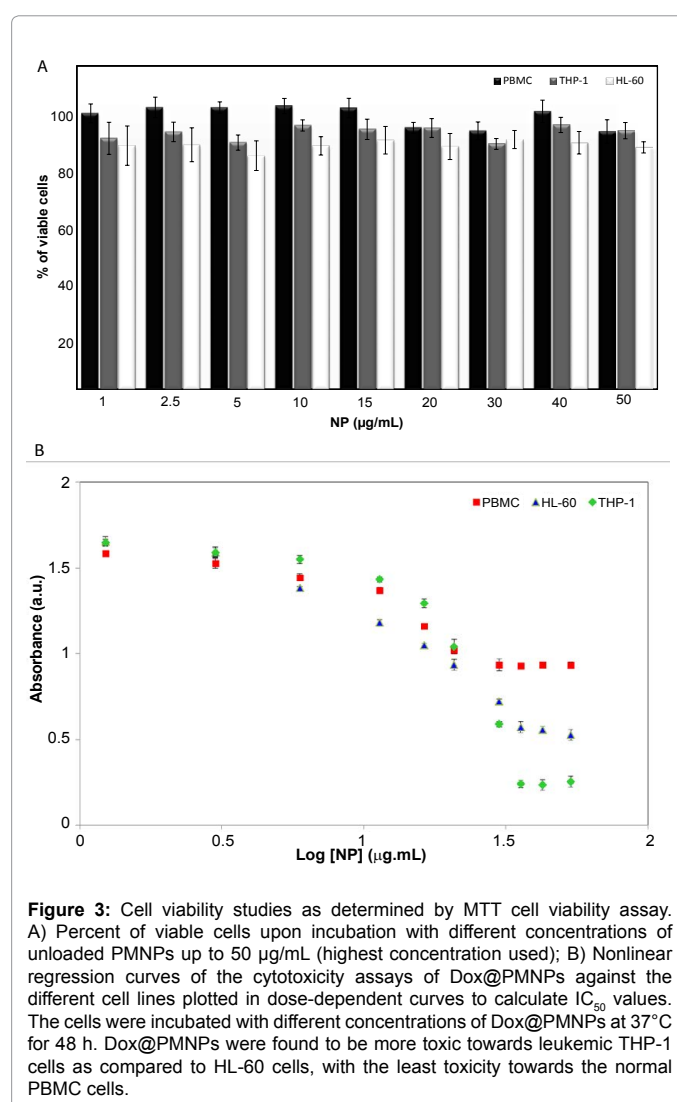
nanocomposites with ~5-10 nm core diameters prepared according to our previously published work [37,38] via the Ko-precipitation Hydrolytic Basic (KHB) methodology (Figure 1). These stable colloidal nanocomposites were selected as carriers for Dox with the intention to develop a theranostic agent for subsequent *in vivo* experiments. We found that the non-covalent interaction and complexation between Dox and the poly-N-vinyl-pyrrolidone (PVP) polymer/NP surface is relatively weak and is pH-dependent, showing several lines of evidence for Dox release from the nanocarriers inside cells. Moreover, the non-covalent conjugation has the advantage of preserving both the structure of the NPs and the attached Dox, enabling intracellular tracking of the drug microscopically. MNPs where drug molecules are covalently conjugated to the NPs' surface usually exhibit low drug entrapment efficiencies and more difficulty in drug release at the target site due to the covalent binding [19]. Furthermore, the orientation of the active functional moieties present in drugs might alter when covalently conjugated [39]. Our studies demonstrated that this simple non-covalent approach formed colloidal water-dispersible drug-loaded PMNP formulations with good loading efficiencies. Up to 60% of the drug was loaded onto PMNPs (i.e., 67  $\mu\text{g}$  of Dox/mg PMNPs), as evident from absorption spectroscopy. Moreover, the obtained nanocolloids were stable for months, without any detectable precipitation or loss of physiochemical properties. The Dox@PMNP nanocarriers prepared were thoroughly characterized by a variety of techniques including transmission electron microscope (TEM), dynamic light scattering (DLS), and thermal gravimetric analyses (TGA) (Figure 2). Respective TEM image of a typical Dox@PMNP dried sample clearly shows 5-10 nm core size diameters. DLS measurements of an aqueous dispersion of Dox@PMNPs in water revealed a hydrodynamic diameter ( $D_H$ )=120 nm with a relatively uniform and narrow size distribution of the as-synthesized particles. No significant changes in the size were observed with time, further confirming the remarkable stability and colloidal nature of the particles in their aqueous dispersions. Furthermore, TGA showed a 39% weight loss of Dox@PMNPs, further confirming the successful adsorption of Dox onto the PMNPs.

With the MNPs in hand, we first sought to test and quantify the toxicities of the as-synthesized NPs towards three different cell lines,



two leukemic and a control normal PBMC cells. In these experiments, the thiazolyl blue tetrazolium bromide (MTT) cell viability assay was used [40]. One of the major advantages of nanoparticulate drug delivery systems is to provide more selective and less harmful solutions to overcome problems of poor specificity and dose-limiting toxicities of active anti-cancer drugs. While the unloaded PMNPs were not toxic to any of the cells, even at the highest NP concentrations tested (50  $\mu\text{g/mL}$ ), Dox@PMNPs were found to be toxic to both leukemic cell lines THP-1 ( $IC_{50}=26.3 \pm 1.7 \mu\text{g/mL}$  NPs corresponding to 3.23  $\mu\text{M}$  Dox) and HL-60 ( $IC_{50}=39.6 \pm 2.1 \mu\text{g/mL}$  NPs corresponding to 4.87  $\mu\text{M}$  Dox), with the least potency towards the normal PBMC cells ( $IC_{50}=155.8 \pm 2.5 \mu\text{g/mL}$  NPs corresponding to 19.2  $\mu\text{M}$  Dox) (Figure 3). Interestingly, Dox@PMNPs showed 6-fold and 4-fold enhanced cytotoxicities against the leukemic cells THP-1 and HL-60 in comparison to the normal PBMC cells, respectively (Figure 4). Importantly, when the cells were treated with free drug at equivalent concentrations, Dox was found to be concurrently toxic to all the three cell lines at comparable inhibitory concentrations (THP-1  $IC_{50}=7.6 \pm 0.75$ , HL-60  $IC_{50}=7.1 \pm 0.76$ , and PBMC  $IC_{50}=7.4 \pm 0.55 \mu\text{M}$  Dox). The observed enhanced cytotoxicities of Dox@PMNPs compared to free Dox against leukemic cells, with the least sensitivity towards the normal PBMC cells suggest huge potentials for the Dox nanocarriers as efficient and selective drug delivery vehicles. We anticipate that the observed enhanced cytotoxic effects of Dox@PMNPs is mostly dependent upon the selective and differential uptake of Dox@PMNPs, and subsequent release of Dox intracellularly due to the biochemical changes inside the cells (mainly pH, hydrolysis, and endosomal/lysosomal hydrolytic enzymes) [41,42]. The payload then translocates to the nucleus in a sustained way exerting its cytotoxic action [38]. Importantly, using the Dox nanocarrier described here is by itself advantageous, as it reduces the unwanted diffusive side effects of the free drug and allows selective targeted drug delivery.

To explore the route of Dox@PMNPs delivery to leukemic cancer cells and perceive the intracellular NP distribution, confocal laser scanning microscopy studies were performed. To mimic physiological conditions, live confocal imaging with no fixation of cells was conducted. We treated two different types of leukemic cells (i.e. THP-1 and HL-60) as well as normal PBMC with Dox alone, PMNPs alone, or Dox@PMNPs, and imaged the cells at different time intervals. The distribution of Dox showed a pattern that varied for cells exposed to free Dox vs Dox@PMNPs. Live confocal images confirmed that Dox is indeed delivered to the cell cytoplasm in relatively short periods



of time (~6 h), but not to the nucleus, due to the intracellular uptake of Dox@PMNPs (Figure 5). Head-to-head comparison between the three cell lines after 24 h of Dox@PMNP incubation showed that Dox was translocated to the nucleus in leukemic cells, with more

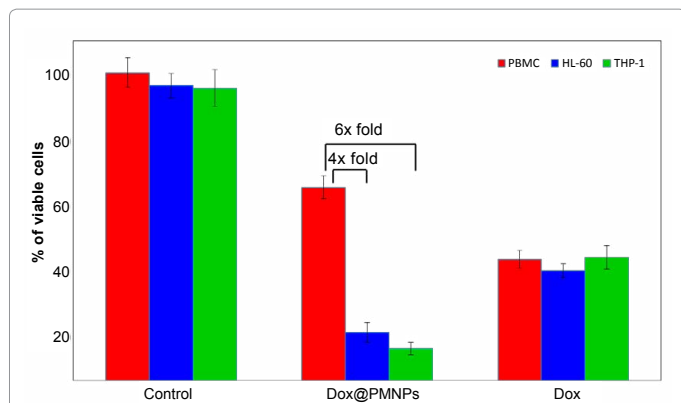


**Figure 4:** MTT plot for the three different human leukemic cell lines treated with either Dox@PMNPs or free Dox at equivalent concentrations. The results noticeably show up to 6-fold increase in potency for the leukemic THP-1 cells compared to the normal PBMC cells. Moreover, in comparison to free Dox, enhanced toxicities of Dox@PMNPs towards the leukemic cell lines is clearly evident, while PBMCs were found to be less sensitive to Dox@PMNPs when compared to free Dox. The obtained results indicate the promising potential for the utilization of Dox@PMNPs for effective and selective drug delivery to human leukemic cancers. The experiments were carried out in triplicate, and error bars denote standard deviations.

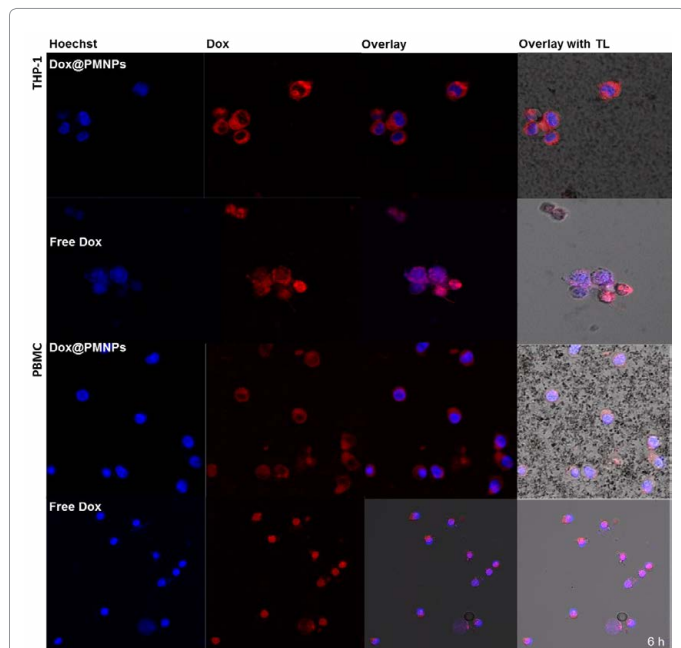


**Figure 5:** Live confocal microscopy images of representative leukemic THP-1 cells (same phenomena observed for HL-60) and normal PBMC cells treated with Dox@PMNPs or equivalent concentration of free Dox for 6 h. Left to right: (a) Blue Hoechst channel showing positions of the nuclei, (b) Red Dox channel, (c) overlay of channels (a) and (b), and (d) overall overlay with transmitted light (TL). Both THP-1 and PBMC cells treated with free Dox showed red Dox fluorescence diffused directly to the nucleus, whereas Dox@PMNPs-treated cells showed Dox signal mostly in the cytoplasm, translocating to the nucleus with time (Figure 6).

intense red fluorescence for THP-1 as compared to HL-60, and typical apoptotic features clearly seen (Figure 6). On the other hand, normal PBMCs showed the least fluorescence intensities, where Dox was found to be mainly in the cytoplasm, with no prominent nuclear staining. These observations excitingly confirmed the cytotoxicity inhibitory concentrations obtained earlier. Moreover, to confirm

this phenomenon further, representative SEM and TEM images of leukemic THP-1 cell line undergoing apoptosis after treatment with Dox@PMNPs for 24 h were recorded (Figures 7 and 8). While SEM clearly shows the change in morphological features as the NPs penetrate the cells delivering Dox, TEM validates the apoptotic features, where the cells curl up, condense and form irregular lumps with membrane blebbings. The NPs were found to be mainly located on the cell membrane and inside the cytoplasm but not in the nucleus. Interestingly, incubating the same cell lines with free Dox at equivalent concentrations, the red fluorescence was found to be directly localized in the nucleus of all cells with minimal detectable presence in the cytoplasm even after only 6 h of incubation. This phenomena is similar to earlier observations by us and others [13,38,43]. It is, thus, repeatedly evident that while free Dox is internalized by passive diffusion through the cell membrane, the uptake of Dox@PMNPs is rather directed by one type of endocytic trafficking mechanisms, specifically micropinocytosis [44,45]. Taking into consideration the distinctive mechanistic cellular uptake between the free drug and drug-loaded NPs (fast diffusion vs vesicular trafficking), our results strongly suggest that Dox@PMNPs can be a promising potential platform for selective drug delivery to human leukemic patients. Moreover, this kind of facile cell labeling of variety of leukemia cells by MNPs suggests that this material may be a good candidate for cellular MRI imaging and tagging of dysfunctional cells. Importantly, this targeted payload is promising to enhance the effectiveness of the drug in leukemic patients and may further allow physicians to image the cells exposed to MNPs. This can potentially open new opportunities for *in vivo* therapeutic imaging and hyperthermia.

## Conclusion

We developed a promising drug-loaded nanocarrier for enhanced and selective Dox delivery to leukemic cells. We have shown that Dox@PMNPs are selectively cytotoxic to human leukemic cells, inducing

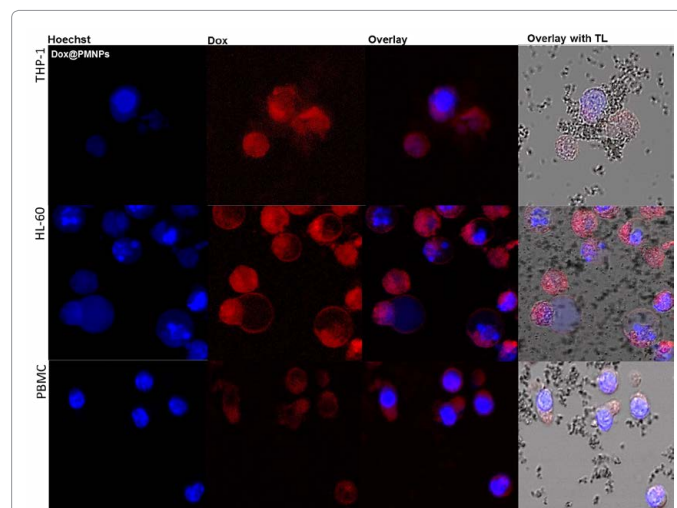


**Figure 6:** Live confocal microscopy images of THP-1, HL-60, and PBMC cells after the same incubation time (24 h) with Dox@PMNPs. Left to right: (a) Blue Hoechst channel showing positions of the nuclei, (b) Red Dox channel, (c) overlay of channels (a) and (b), and (d) overall overlay with TL. Images show that Dox@PMNPs are internalized more inside THP-1 compared to HL-60, causing apoptosis to both cells (typical apoptotic features such as condensation, shrinking, and irregular lump formation with membrane blebbing are clearly seen in the overlaid picture). Nonetheless for normal PBMCs, and even after 24 h of incubation, the red fluorescence was only apparent in the cytoplasm, but not in the nucleus, suggesting huge potentials for Dox@PMNPs as selective anticancer vehicles for leukemic cells.

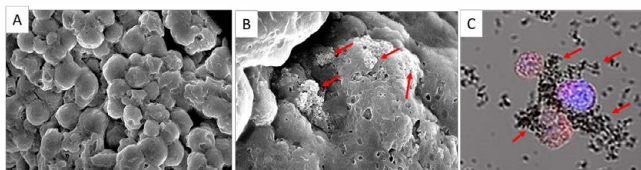


**Figure 7:** SEM images of representative leukemic THP-1 cell line after treatment with Dox@PMNPs for 24 h. (a) THP-1 cells without NPs, (b) NP-treated THP-1 cells, and (c) confocal microscopy image of the corresponding NP-treated THP1 cells. Red arrows clearly show the NPs on the cell surface and penetrating the cells changing the morphological features of the cells.

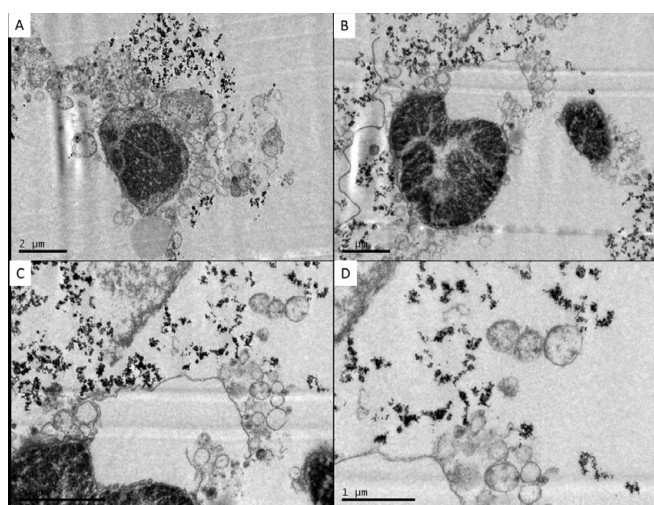


**Figure 8:** Representative leukemic THP-1 cell line undergoing apoptosis after treatment with Dox@PMNPs for 24 h, as captured by TEM microscopy at different magnifications. The apoptotic features, where the cancerous cells curl up, condense and form irregular lumps with membrane blebbing are clearly evident. The NPs were found to be mainly located on the cell membrane and inside the cytoplasm but not in the nucleus.

apoptotic cell death to THP-1 and HL-60 cells, with the least sensitivity towards normal PBMCs. On the other hand, when treated alone, free Dox is found to be concurrently less toxic to all the cell lines tested, suggesting huge potentials for Dox@PMNPs to be utilized as selective anticancer agents for leukemic cancer therapy. From the microscopy results, it is clear that Dox@PMNPs are endocytosed inside the cell cytoplasm, releasing the toxic drug payload intracellularly and causing apoptotic cell death. The prepared nanomedical formulation established here can potentially open new opportunities for *in vivo* therapeutic imaging, cancer monitoring, and hyperthermia.

#### Acknowledgments

This work was funded by KAIMRC through Grant RC13/204/R. The author acknowledges the continuous support by KSAU-HS, NGHHA, and the core facility at KAIMRC. The authors also thank Hajar Al-Zahrani (cell culture), and Thadeo Trivilegio (PBMC preparation) for their assistance and help in the study as indicated.

#### Notes

The authors declare no competing financial interest.

#### References

1. Barenholz Y (2012) Doxil®—The first FDA-approved nano-drug: lessons learned. J Control Release 160: 117-134.
2. Smith JA, Costales AB, Jaffari M, Urbauer DL, Frumovitz M, et al. (2015) Is it equivalent? Evaluation of the clinical activity of single agent Lipodox®

compared to single agent Doxil® in ovarian cancer treatment. J Oncol Pharm Pract 22: 599-604.

3. Rivankar S (2014) An overview of doxorubicin formulations in cancer therapy. J Cancer Res Ther 10: 853-858.
4. Wickham T, Futch K (2012) A phase I study of MM-302, a HER2-targeted liposomal doxorubicin, in patients with advanced, HER2-positive breast cancer. Cancer Res 72: P5-18-09.
5. Jain RK, Stylianopoulos T (2010) Delivering nanomedicine to solid tumors. Nat Rev Clin Oncol 7: 653-664.
6. Duncan R (2006) Polymer conjugates as anticancer nanomedicines. Nat Rev Cancer 6: 688-701.
7. Min Y, Caster JM, Eblan MJ, Wang AZ (2015) Clinical Translation of Nanomedicine. Chem Rev 115: 11147-11190.
8. Huang J, Li Y, Orza A, Lu Q, Guo P, et al. (2016) Magnetic Nanoparticle Facilitated Drug Delivery for Cancer Therapy with Targeted and Image-Guided Approaches. Adv Funct Mater 26: 3818-3836.
9. Ren Y, Zhang H, Chen B, Cheng J, Cai X, et al. (2012) Multifunctional magnetic Fe<sub>3</sub>O<sub>4</sub> nanoparticles combined with chemotherapy and hyperthermia to overcome multidrug resistance. Int J Nanomedicine 7: 2261-2269.
10. Chen B, Cheng J, Shen M, Gao F, Xu W, et al. (2009) Magnetic nanoparticle of Fe<sub>3</sub>O<sub>4</sub> and 5-bromotetrandrin interact synergistically to induce apoptosis by daunorubicin in leukemia cells. Int J Nanomedicine 4: 65-71.
11. Cheng J, Wang J, Chen B, Xia G, Cai X, et al. (2011) A promising strategy for overcoming MDR in tumor by magnetic iron oxide nanoparticles co-loaded with daunorubicin and 5-bromotetrandrin. Int J Nanomedicine 6: 2123-2131.
12. Wang J, Chen B, Cheng J, Cai X, Xia G, et al. (2011) Apoptotic mechanism of human leukemia K562/A02 cells induced by magnetic iron oxide nanoparticles co-loaded with daunorubicin and 5-bromotetrandrin. Int J Nanomedicine 6: 1027-1034.
13. El-Dakdouki MH, Zhu DC, El-Boubbou K, Kamat M, Chen J, et al. (2012) Development of multifunctional hyaluronan-coated nanoparticles for imaging and drug delivery to cancer cells. Biomacromolecules 13: 1144-1151.
14. Jain TK, Richey J, Strand M, Leslie-Pelecky DL, Flask CA, et al. (2008) Magnetic nanoparticles with dual functional properties: Drug delivery and magnetic resonance imaging. Biomaterials 29: 4012-4021.
15. Dobson J (2006) Magnetic nanoparticles for drug delivery. Drug Dev Res 67: 55-60.
16. Sun C, Lee JSH, Zhang M (2008) Magnetic nanoparticles in MR imaging and drug delivery. Adv Drug Deliv Rev 60: 1252-1265.
17. Ulbrich K, Holá K, Šubr V, Bakandritsos A, Tuček J, et al. (2016) Targeted Drug Delivery with Polymers and Magnetic Nanoparticles: Covalent and Noncovalent Approaches, Release Control, and Clinical Studies. Chem Rev 116: 5338-5431.
18. Sajja HK, East MP, Mao H, Wang YA, Nie S, et al. (2009) Development of multifunctional nanoparticles for targeted drug delivery and noninvasive imaging of therapeutic effect. Curr Drug Discovery Technol 6: 43-51.
19. Laurent S, Saei AA, Behzadi S, Panahifar A, Mahmoudi M (2014) Superparamagnetic iron oxide nanoparticles for delivery of therapeutic agents: opportunities and challenges. Expert Opin Drug Deliv 11: 1449-1470.
20. Xie J, Liu G, Eden HS, Ai H, Chen X (2011) Surface-Engineered Magnetic Nanoparticle Platforms for Cancer Imaging and Therapy. Acc Chem Res 44: 883-892.
21. Estelrich J, Escibano E, Queralto J, Busquets MA (2015) Iron Oxide Nanoparticles for Magnetically-Guided and Magnetically-Responsive Drug Delivery. Int J Mol Sci 16: 8070-8101.
22. Wahajuddin M, Arora S (2012) Superparamagnetic iron oxide nanoparticles: magnetic nanoplatforms as drug carriers. Int J Nanomedicine 7: 3445-3471.
23. Yu MK, Jeong YY, Park J, Park S, Kim JW, et al. (2008) Drug-loaded superparamagnetic iron oxide nanoparticles for combined cancer imaging and therapy in vivo. Angew Chem Int Ed 47: 5362-5365.
24. Arruebo M, Fernández-Pacheco R, Ibarra MR, Santamaría J (2007) Magnetic nanoparticles for drug delivery. Nano Today 2: 22-32.

25. Chen BA, Dai YY, Wang XM, Zhang RY, Xu WL, et al. (2008) Synergistic effect of the combination of nanoparticulate Fe<sub>3</sub>O<sub>4</sub> and Au with daunomycin on K562/A02 cells. *Int J Nanomedicine* 3: 343-350.
26. Cheng J, Cheng L, Chen B, Xia G, Gao C, et al. (2012) Effect of magnetic nanoparticles of Fe<sub>3</sub>O<sub>4</sub> and wogonin on the reversal of multidrug resistance in K562/A02 cell line. *Int J Nanomedicine* 7: 2843-2852.
27. Chen B, Liang Y, Wu W, Cheng J, Xia G, et al. (2009) Synergistic effect of magnetic nanoparticles of Fe<sub>3</sub>O<sub>4</sub> with gambogic acid on apoptosis of K562 leukemia cells. *Int J Nanomedicine* 4: 251-259.
28. Zhang G, Lai BB, Zhou YY, Chen BA, Wang XM, et al. (2011) Fe<sub>3</sub>O<sub>4</sub> nanoparticles with daunorubicin induce apoptosis through caspase 8-PARP pathway and inhibit K562 leukemia cell-induced tumor growth in vivo. *Nanomedicine* 7: 595-603.
29. Zhang R, Wu C, Wang X, Sun Q, Chen B, et al. (2009) Enhancement effect of nano Fe<sub>3</sub>O<sub>4</sub> to the drug accumulation of doxorubicin in cancer cells. *Mater Sci Eng C* 29: 1697-1701.
30. Kassab E, Darwish M, Timsah Z, Liu S, Leppla SH, et al. (2013) Cytotoxicity of Anthrax Lethal Toxin to Human Acute Myeloid Leukemia Cells Is Nonapoptotic and Dependent on Extracellular Signal-Regulated Kinase 1/2 Activity. *Transl Oncol* 6: 25-32.
31. Centelles JJ (2014) Treatment of Acute Myeloid Leukemia. *Curr Synthetic Sys Biol* 2: 114.
32. Bekdash A, Darwish M, Timsah Z, Kassab E, Ghanem H, et al. (2015) Phospho-MEK1/2 and uPAR Expression Determine Sensitivity of AML Blasts to a Urokinase-Activated Anthrax Lethal Toxin (PrAgU2/LF). *Transl Oncol* 8: 347-357.
33. Qin Z (2012) The use of THP-1 cells as a model for mimicking the function and regulation of monocytes and macrophages in the vasculature. *Atherosclerosis* 221: 2-11.
34. Kamat M, El-Boubbou K, Zhu DC, Lansdell T, Lu X, et al. (2010) Hyaluronic acid immobilized magnetic nanoparticles for active targeting and imaging of macrophages. *Bioconjugate Chem* 21: 2128-2135.
35. Sun H, Wang Y (1995) Apoptosis of human leukemic HL-60 cells induced to differentiate by treatment with RA or DMSO. *Cell Research* 5: 181-186.
36. El-Boubbou K, Al-Kaysi RO, Al-Muhanna MK, Bahhari HM, Al-Romaeh AI, et al. (2015) Ultra-Small Fatty Acid-Stabilized Magnetite Nanocolloids Synthesized by In Situ Hydrolytic Precipitation. *Journal of Nanomaterials Article ID 620672*: 11.
37. El-Boubbou K, Ali R, Bahhari HM, AlSaad KO, Nehdi A, et al. (2016) Magnetic Fluorescent Nanoformulation for Intracellular Drug Delivery to Human Breast Cancer, Primary Tumors, and Tumor Biopsies: Beyond Targeting Expectations. *Bioconjugate Chem* 27: 1471-1483.
38. Li SD, Huang L (2008) Pharmacokinetics and Biodistribution of Nanoparticles. *Mol Pharmaceutics* 5: 496-504.
39. Mosmann T (1983) Rapid colorimetric assay for cellular growth and survival: Application to proliferation and cytotoxicity assays. *Journal of Immunological Methods* 65: 55-63.
40. Vivek R, Thangam R, NipunBabu V, Rejeeth C, Sivasubramanian S, et al. (2014) Multifunctional HER2-Antibody Conjugated Polymeric Nanocarrier-Based Drug Delivery System for Multi-Drug-Resistant Breast Cancer Therapy. *ACS Appl Mater Interfaces* 6: 6469-6480.
41. Bennet D, Kim S (2014) Polymer Nanoparticles for Smart Drug Delivery. *Nanotechnology and Nanomaterials: Application of Nanotechnology in Drug Delivery*.
42. Yang X, Grailer JJ, Rowland IJ, Javadi A, Hurley SA, et al. (2010) Multifunctional Stable and pH-Responsive Polymer Vesicles Formed by Heterofunctional Triblock Copolymer for Targeted Anticancer Drug Delivery and Ultrasensitive MR Imaging. *ACS Nano* 4: 6805-6817.
43. Sahay G, Alakhova DY, Kabanov AV (2010) Endocytosis of Nanomedicines. *J Control Release* 145: 182-195.
44. Rejman J, Oberle V, Zuhorn IS, Hoekstra D (2004) Size-dependent internalization of particles via the pathways of clathrin- and caveolae-mediated endocytosis. *Biochem J* 377: 159-169.
45. Tawil M, Bekdash A, Mroueh M, Daher CF, Abi-Habib RJ (2015) Wild carrot oil extract is selectively cytotoxic to human acute myeloid leukemia cells. *Asian Pac J Cancer Prev* 16: 761-767.